Electron Acceleration Mechanisms in the Interaction of Ultrashort Lasers with Underdense Plasmas: Experiments and Simulations

J. Faure[*†], E. Lefebvre[**], V. Malka[‡†], J.-R. Marquès[†], F. Amiranoff[†], A. Solodov[§] and P. Mora[§]

[*]*Lawrence Berkeley National Laboratory, University of California, Berkeley, CA 94720*
[†]*Laboratoire pour l'Utilisation des Lasers Intenses, École Polytechnique, 91128 Palaiseau, France*
[**]*CEA, Bruyères le Chatel, France*
[‡]*Laboratoire d'Optique Appliquée, ENSTA, 91128 Palaiseau, France*
[§]*Centre de Physique Théorique, École Polytechnique, 91128 Palaiseau, France*

Abstract. An experiment investigating the production of relativistic electrons from the interaction of ultrashort multi-terawatt laser pulses with an underdense plasma is presented. Electrons were accelerated to tens of MeV and the maximum electron energy increased as the plasma density decreased. Simulations have been performed in order to model the experiment. They show a good agreement with the trends observed in the experiment and the spectra of accelerated electrons could be reproduced successfully. The simulations have been used to study the relative contribution of the different acceleration mechanisms: plasma wave acceleration, direct laser acceleration and stochastic heating. The results show that in the low density case (1% of the critical density), acceleration by plasma waves dominates whereas in the high density case (10% of the critical density) acceleration by the laser is the dominant mechanism. The simulations at high density also suggest that direct laser acceleration is more efficient than stochastic heating.

1. INTRODUCTION

The relativistic interaction of an ultrashort, multi-terawatt laser with an underdense plasma can result in the generation of a bright electron source [1, 2]. Typically, about 10^{11} electrons are accelerated and expelled out of the plasma. The electron energy distribution is Maxwellian-like, with a few electrons reaching tens of MeV energies. Such a source could be of interest for a variety of applications including nuclear activation [3, 4], the generation of bright and/or ultrashort radiation sources, such as X-ray sources [5, 6, 7] or THz sources [8]. Also relevant is the fact that the electron source (and the subsequent radiation sources it can generate) is perfectly synchronized with the laser which created it. This makes it a novel and extremely useful scientific tool as it could be used for pump probe experiments in many different fields.

In order to improve and optimize this source, it is necessary to fully understand the underlying and complex physics responsible for the acceleration of the electrons. In the past years, there has been a controversy on the subject and several scenarios have been proposed to explain the trapping and the acceleration of the plasma electrons. The first

possible scenario is wavebreaking [9, 10]: as the laser interacts with the plasma, the interplay of self-focusing [11, 12], Raman forward scattering [13] and self-modulation [14, 15] causes the creation of a relativistic plasma wave. For sufficiently large waves, longitudinal electric fields can reach $\sim 100\,\mathrm{GV/m}$, resulting in trapping of background plasma electrons and acceleration of these electrons to multi-MeV energies. This mechanism relies on the plasma as the accelerating structure, however, other mechanisms have recently been proposed where the acceleration comes from the laser itself. An example of laser acceleration is betatron acceleration or Direct Laser Acceleration (DLA) [16, 17]. In this mechanism, the laser creates a plasma channel through the radial ponderomotive force, electrons oscillate at the betatron frequency in this channel and when the betatron frequency coincides with the laser frequency in the electron frame, a resonance occurs and energy can be transferred from the laser to the electrons. This mechanism could explain the acceleration of electrons as witnessed in experiments [18]. Finally, stochastic heating [19] is another mechanism which could explain the experiments. In this case, electron acceleration is due to the stochastic motion of electrons in two counter-propagating strong electromagnetic fields. The counter-propagating laser field could simply come from Raman backward scattered waves which trigger stochastic motion when they reach sufficiently high amplitudes. Recent Particle In Cell (PIC) simulations [20] showed that acceleration to tens of MeV is also possible with this mechanism.

The goal of this paper is to estimate the contribution of each of these mechanisms in a recent electron acceleration experiment [21]. The details of the interaction are hard to infer from experimental observables and simulations are necessary to gain some insight on the physics of the acceleration. Hence in section 2 we will first summarize the experimental results which will be used as a test bed to benchmark our codes. Two codes have been used to model the experiment: the code WAKE [22] and a 2D PIC code [23]. In section 3 we will show the results of the simulations.

2. SUMMARY OF THE EXPERIMENTAL RESULTS

The experiments were performed at *Laboratoire d'Optique Appliquée* and were described in detail in Ref. [21, 24, 25]. The 10 Hz, 800 nm laser delivered up to 600 mJ in 35 fs. It was focused to a waist of $w_0 = 6\,\mu\mathrm{m}$, and intensities up to $I = 1.8\times10^{19}\,\mathrm{W/cm^2}$ could be reached. The laser was focused onto the edge of a supersonic Helium gas jet. Electron densities from $n_e = 10^{19}\,\mathrm{cm^{-3}}$ to $1.5\times10^{20}\,\mathrm{cm^{-3}}$ could be obtained by changing the backing pressure of the jet. Electron energies from 0 to 200 MeV could be measured using an magnetic electron spectrometer. The total number of electrons was measured using a commercial Integrated Charge Transformer (ICT). More details can be found in [21].

On Fig. 1a is picture of the electron spectra obtained for two different densities: $n_e = 5\times10^{19}\,\mathrm{cm^{-3}}$ and $1.5\times10^{20}\,\mathrm{cm^{-3}}$. The distribution is Maxwell-like and can be fitted by an exponential function of the form $\exp[-E/T_{eff}]$, where E is the electron energy and T_{eff} the effective temperature of the distribution. The maximum energy E_{max} is defined as the intersection of the exponential fit with the detection threshold. While

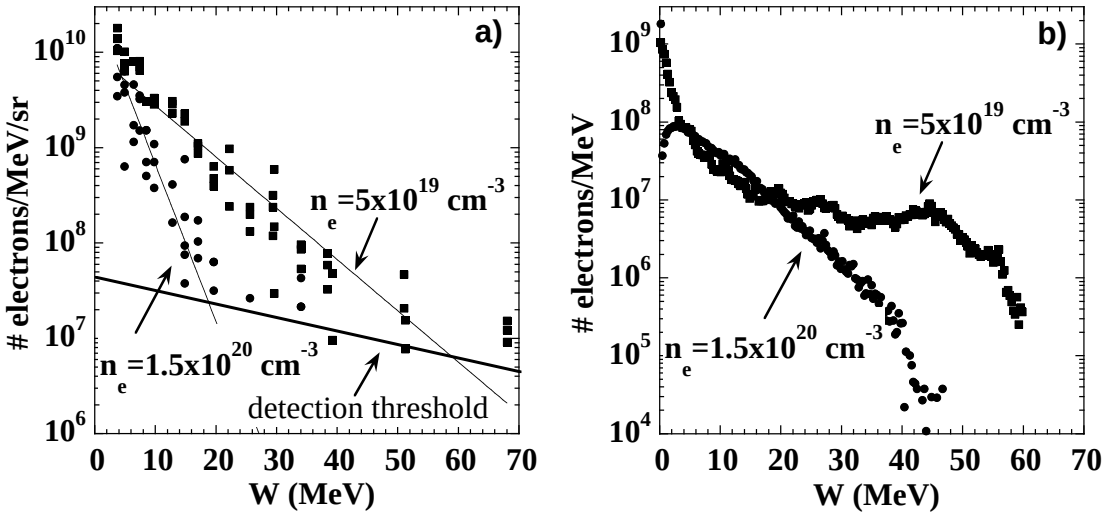

FIGURE 1. a): Experimental electron spectra obtained for $n_e = 5 \times 10^{19}\,\mathrm{cm}^{-3}$ and $1.5 \times 10^{20}\,\mathrm{cm}^{-3}$. Laser parameters were $I = 1.8 \times 10^{19}\,\mathrm{W/cm}^2$, $\tau = 35\,\mathrm{fs}$, $w_0 = 6\,\mu\mathrm{m}$. b): PIC simulation of the electron spectra for the same physical parameters.

this value depends on the detection threshold, it is a good parameter that represents the behavior of the distribution. As can be seen on Fig. 1, both T_{eff} and E_{max} increase when the density decreases. This behavior is consistent for all electron densities as can be seen on Fig. 2a. Figure 2b also shows that E_{max} increases when the intensity increases (the intensity can be changed either by increasing the pulse duration of by decreasing the pulse energy).

Although the dependence of electron spectra on laser and plasma parameters does not indicate directly which mechanisms dominate, we next discuss the experimental results and see how they relate to theory. Simple scaling laws exist in the case of acceleration by plasma waves [26, 27]; the maximum energy an electron can gain in a plasma wave is given by

$$E_{max} = 4 m_e c^2 \gamma_p^2 \frac{\delta n}{n} \gamma_\perp^{3/2} \tag{1}$$

where $\delta n/n$ is the amplitude of the plasma wave and $\gamma_p = (1 - v_p^2/c^2)^{-1/2}$ is the relativistic factor associated with the phase velocity of the plasma wave v_p. $\gamma_\perp = (1 + a_0^2/2)^{1/2}$ is the relativistic factor associated to the quivering motion of the electrons in the laser field, a_0 being the normalized vector potential of the laser field. The factor 4 in the right hand side of Eq. (1) comes from the assumption that a plasma channel, created by the radial ponderomotive force, exists. In this case all phases are focusing [27]. The amplitude of the plasma wave has not been measured in our experiment but we assumed $\delta n/n = 20\%$. This assumption is somewhat arbitrary but when compared with the experiment, this simple scaling law correctly reproduces the observed behavior: this is shown on Fig. 2 where the full curves represent the scaling law.

However, reality might be more complicated than these simple estimates. Although no simple scaling exists for DLA, it has been shown [16] that the temperature of the electron distribution increases as $I^{1/2}$, which is close to the behavior of our experiment. Similarly,

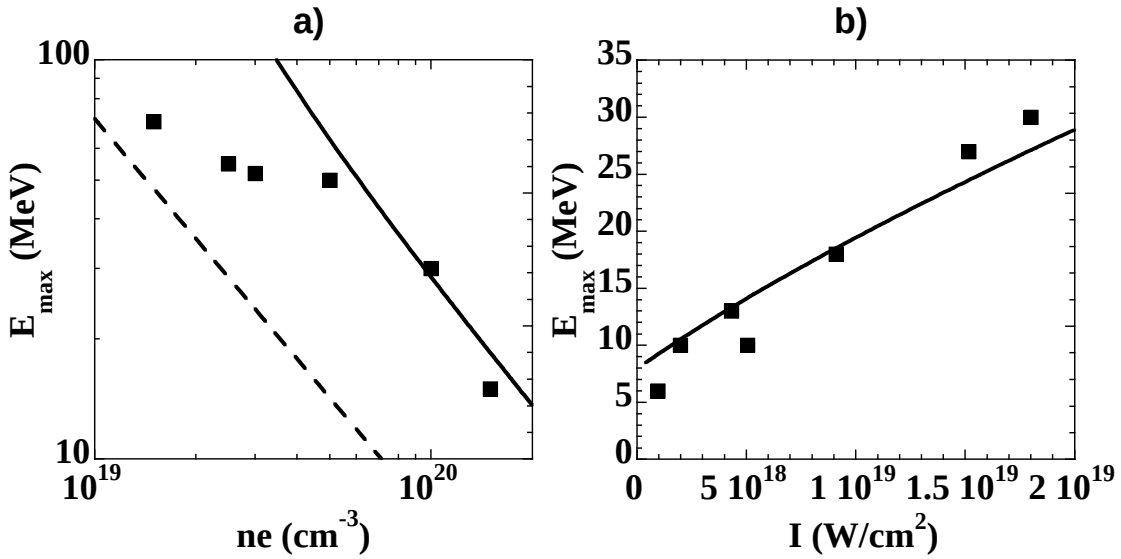

FIGURE 2. a): Variation of electron maximum energy as a function of density for $I = 1.8 \times 10^{19}\,\mathrm{W/cm^2}$, $\tau = 35\,\mathrm{fs}$. Squares: experimental points. The full line corresponds to the scaling law (acceleration by plasma waves) with relativistic correction; the dashed line to the scaling law without relativistic correction. In both cases, $\delta n/n = 20\%$. b): Variation of electron maximum energy with laser intensity at $n_e = 10^{20}\,\mathrm{cm^{-3}}$. Squares: experimental points. The full line correspond to the scaling law with relativistic corrections.

simulations in Ref. [17] show that the maximum energy is higher for lower plasma densities. As a consequence, DLA also satisfies the trend observed in our experiments. As for stochastic heating, a simple scaling derived from 1D PIC simulations in Ref. [20] is $T_{eff} \sim a_0 a_1^{1/2}$, where a_1 is the normalized potential vector of the reflected field. According to this scaling, one would expect stochastic heating to be less efficient when the density is lower: at low density, Raman backward scattering is less efficient and as a consequence a_1 is smaller. This is opposite from what has been observed in experiments and one can expect stochastic heating to be of minor importance at lower electron density.

3. WAKE AND 2D PIC SIMULATIONS

To quantify and understand better the details of the interaction, we now present results of simulations with WAKE and a 2D PIC code, modeling the experiment. Both codes are able to reproduce the trends of Fig. 2. However, WAKE systematically overestimates the energy gain of accelerated electrons. The reasons are the following: (i) in WAKE, longitudinal wavebreaking is not described. As a consequence, the amplitude of the plasma waves is overestimated. (ii) Accelerated electrons are modeled by test electrons which are pushed in the fields calculated by WAKE. Thus, beamloading effects are ignored which also leads to an overestimation of the plasma fields. Finally, approximations in the code limit the laser power to a few P_c (critical power for self-focusing). Hence, only

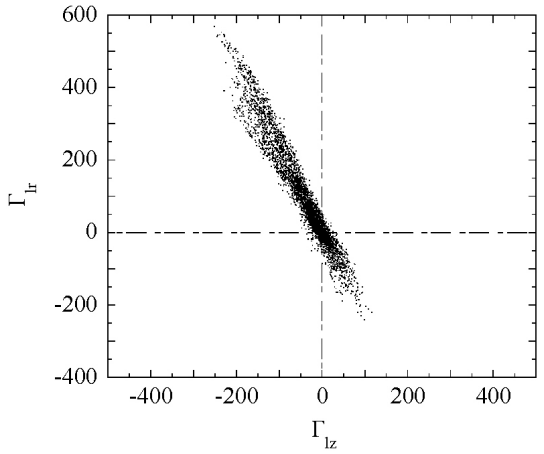

FIGURE 3. Result of a WAKE simulation with $I = 1.8 \times 10^{19}\,\mathrm{W/cm^2}$, $\tau = 35\,\mathrm{fs}$, $w_0 = 6\,\mu\mathrm{m}$ and $n_e = 2 \times 10^{19}\,\mathrm{cm^{-3}}$. Each point in the plane (Γ_{lz}, Γ_{lr}) represents an accelerated test electron after a propagation distance of $z = 7.5 z_R$. The plot shows the relative contribution of the longitudinal and transverse laser fields.

the low density cases could be modeled correctly (up to $2 \times 10^{19}\,\mathrm{cm^{-3}}$). However, as we will see later, WAKE has advantages over a PIC code.

The 2D PIC code not only reproduces the trend of the experiment but gives results quantitatively comparable to the experiment in terms of number of accelerated electrons (several nC), and shape of the electron spectra. Fig. 1b represents simulated spectra obtained with parameters corresponding to the experiment.

In order to separate the contribution of acceleration by plasma waves and acceleration by the laser, the following integrals have to be estimated

$$\Gamma_{p,l} = -\int_0^t \frac{e\mathbf{E}_{p,l} \cdot \mathbf{v}}{m_e c^2} dt \tag{2}$$

Γ_p and Γ_l represent respectively the work that plasma fields $\mathbf{E}_p$ and laser fields $\mathbf{E}_l$ exert on electrons. This is different from what has been done in Ref. [18], where the following integrals were estimated

$$\Gamma_{r,z} = -\int_0^t \frac{e\mathbf{E}_{r,z} \cdot \mathbf{v}}{m_e c^2} dt \tag{3}$$

where Γ_r and Γ_z represent respectively the work that transverse fields $\mathbf{E}_r$ and longitudinal fields $\mathbf{E}_z$ exert on electrons. In Ref. [18], the transverse and longitudinal fields were assumed to be the laser and plasma fields, respectively. However this is not exact since laser fields have both transverse and longitudinal components: $\mathbf{E}_l = \mathbf{E}_{lr} + \mathbf{E}_{lz}$. The same holds for plasma fields: $\mathbf{E}_p = \mathbf{E}_{pr} + \mathbf{E}_{pz}$. Thus the quantities $\Gamma_{r,z}$ both mix laser and plasma fields.

In order to illustrate the difference between the two integrals, we used the code WAKE. In WAKE, both Eq. (2) and (3) can be estimated because the code solves separate equations for the laser and the plasma fields. The simulation was done with parameters corresponding to the experiment and $n_e = 2 \times 10^{19}\,\mathrm{cm^{-3}}$. A bunch of 3×10^4

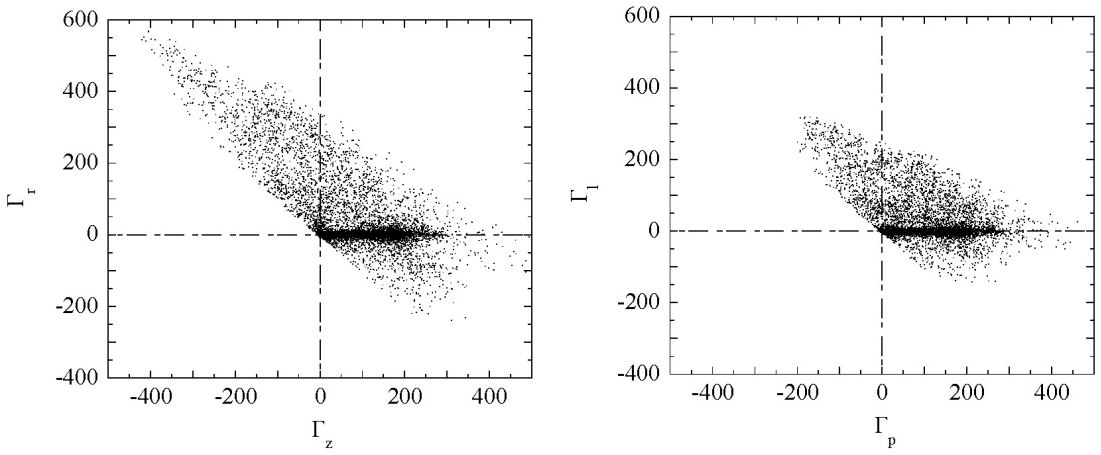

FIGURE 4. Result of a WAKE simulation with $I = 1.8 \times 10^{19}\,\mathrm{W/cm^2}$, $\tau = 35\,\mathrm{fs}$, $w_0 = 6\,\mu\mathrm{m}$ and $n_e = 2 \times 10^{19}\,\mathrm{cm^{-3}}$. Comparison between two representations of the accelerated test electrons: in the plane (Γ_p, Γ_l) (right picture) and in the plane (Γ_z, Γ_r) (left picture).

test electrons was injected after one Rayleigh length of laser propagation. Fig. 3 shows accelerated electrons in a diagram (Γ_{lz}, Γ_{lr}), representing the respective contribution of the longitudinal and transverse laser fields. This picture shows clearly that the action of the longitudinal laser field cannot be ignored: as the transverse field accelerates electrons by 250 MeV, the longitudinal field decelerates them by 100 MeV.

On Fig. 4, we compare the integrals from Eq. (2) and (3). The picture on the right shows electrons in the plane (Γ_p, Γ_l) which is the correct representation for separating the contributions of the laser and of the plasma. The picture on the left represents electrons in the plane (Γ_z, Γ_r). As can be seen on Fig. 4, if one interprets Γ_z as the contribution from the plasma and Γ_r as the contribution from the laser, one overestimates the acceleration by the laser. However, in this particular case, the two diagnostics do not contradict each other and they both show that although acceleration by the laser cannot be neglected, the acceleration by plasma waves dominates.

In a PIC code, separating the laser field from the plasma field is a very complicated problem. Thus from now on, we will restrict ourselves to evaluating the integrals of Eq. (3), keeping in mind that their interpretation might be difficult. Nevertheless the use of the PIC code is necessary to model our experimental parameters as well as phenomena such as wavebreaking and beamloading. On Fig. 5, the accelerated electrons produced after two Rayleigh lengths are represented in the plane (Γ_z, Γ_r) for different densities. As the figure shows, at lower density ($5 \times 10^{19}\,\mathrm{cm^{-3}}$ top left picture), $\mathbf{E}_z$ is the dominant accelerating field although $\mathbf{E}_r$ also plays a role in the acceleration. At high density ($1.5 \times 10^{20}\,\mathrm{cm^{-3}}$ bottom right picture), the acceleration seems to be dominated by $\mathbf{E}_r$ fields. In fact, this last picture is very close to Fig. 3 and seems to indicate that at large density, laser acceleration largely dominates. The $\mathbf{E}_z$ part would then be due almost only to the longitudinal laser field. This statement is supported by the fact that in the high density simulations, the density plots do not show any plasma wave structure. In summary, Fig. 5 suggests that at high density the main acceleration comes from the laser whereas at lower density, it comes from the plasma waves.

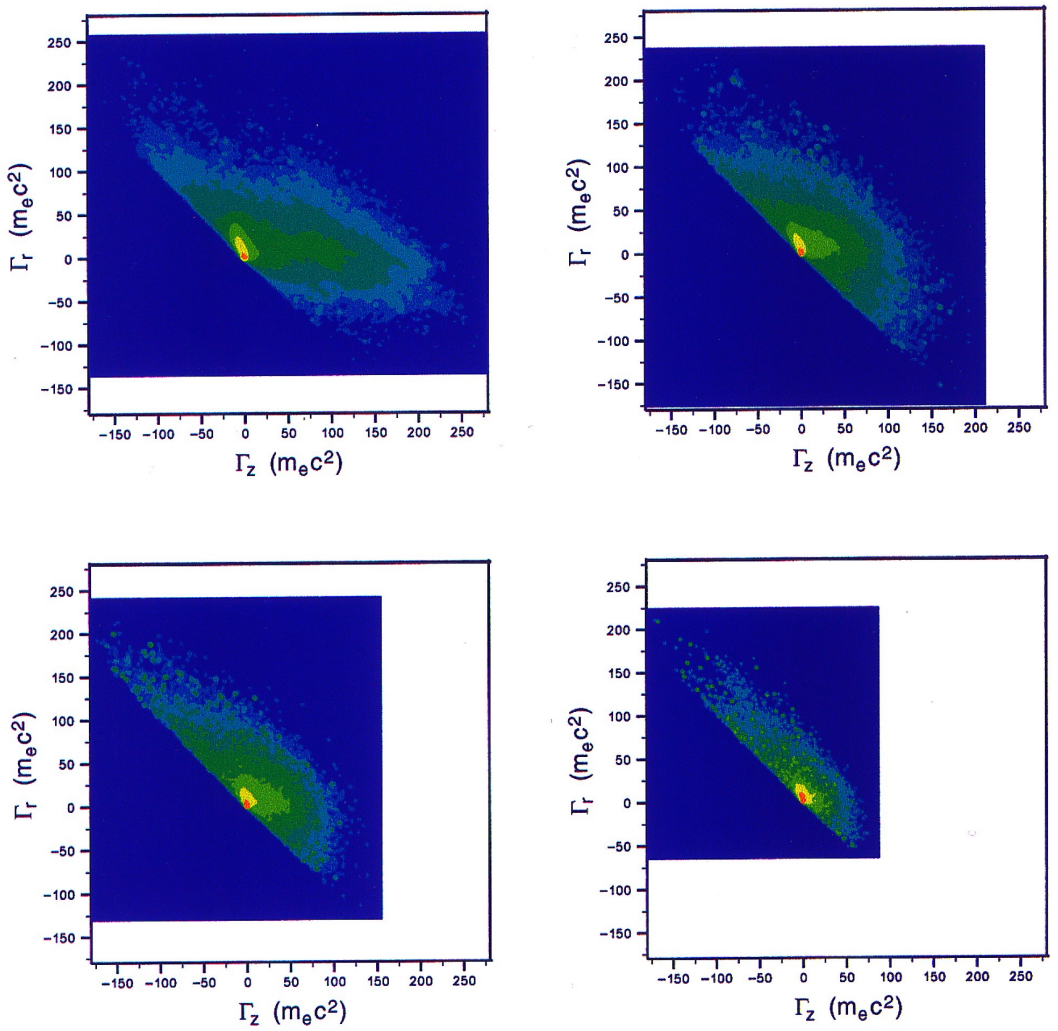

FIGURE 5. Results of 2D PIC simulations. Representation of electrons accelerated in the plane (Γ_z, Γ_r) after $z = 2z_R$ and for several electron densities. Top left: $5 \times 10^{19}\,\mathrm{cm}^{-3}$, top right: $6.4 \times 10^{19}\,\mathrm{cm}^{-3}$, bottom left: $10^{20}\,\mathrm{cm}^{-3}$, bottom right: $1.5 \times 10^{20}\,\mathrm{cm}^{-3}$

A question still remains unanswered: at high density, when acceleration by the laser dominates, what is the mechanism responsible for electron acceleration: stochastic heating or direct laser acceleration? This question can be answered by using the 2D PIC code: when running the code with the laser polarization out of the simulation plane (s-polarization), electrons cannot be accelerated through DLA because their motion is perpendicular to the transverse electric field. In this case, the DLA mechanism is suppressed and acceleration comes mainly from stochastic heating. On the contrary, in p-polarization (the laser is then polarized in the plane of the simulation), DLA is possible, as well as stochastic heating. Thus, if simulations with s and p polarization produce different results, it will give insight on the acceleration mechanisms. The results are shown on Fig. 6: the left picture shows the electron distributions obtained in the high

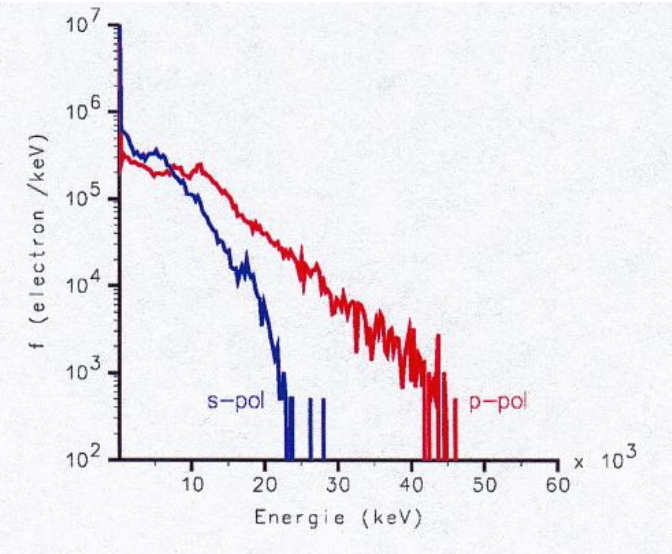

FIGURE 6. Results of 2D PIC code. Electron distributions for runs where the laser was s or p-polarized. $n_e = 1.5 \times 10^{20}\,\mathrm{cm}^{-3}$.

density case ($1.5 \times 10^{20}\,\mathrm{cm}^{-3}$). The picture suggests that DLA is indeed present in the run with p-polarization since the distribution extends to 40 MeV instead of 20 MeV in the s-polarization case[1]. DLA being a resonant mechanism is probably more efficient than stochastic heating, which would explain the difference. Density plots also show the formation of a strong density depression inside the laser pulse. This could provide the plasma channel relevant for the DLA mechanism.

4. CONCLUSION

In conclusion, both experiments and simulations show that electrons are accelerated to higher energies at low plasma electron densities. WAKE and 2D PIC simulations indicate that at low density, acceleration by plasma waves is the dominant mechanism. This shows that an efficient laser-plasma based accelerator should operate at low density in order to take advantage of the acceleration by plasma waves, the most efficient mechanism.

WAKE simulations showed that in general, the contribution of the longitudinal laser field should not be neglected since it tends to decelerate particles. These simulations also showed that one should be cautious when trying to interpret (Γ_z, Γ_r) diagrams especially since Γ_z contains contributions from both laser and plasma fields.

Finally, the (Γ_z, Γ_r) diagrams produced with the 2D PIC code showed that at high plasma density (10% of critical density), electron acceleration is mainly due to the laser.

[1] The dramatic difference between simulations with s or p polarization suggests that the 3D geometry is really necessary to fully model the problem.

The results also indicate that both stochastic heating and DLA could play a role, although DLA seems to be a more efficient mechanism.

ACKNOWLEDGMENTS

The authors wish to acknowledge the support of the laser team at *Laboratoire d'Optique Appliquée*. They also acknowledge useful discussions with A. Pukhov, W. Mori, E. Esarey, C. Schroeder and W. Leemans.

REFERENCES

1. Modena, A., Dangor, A., Najmudin, Z., Clayton, C., Marsh, K., Joshi, C., Malka, V., Darrow, C., Neely, D., and Walsh, F., *Nature*, **377**, 606–608 (1995).
2. Umstadter, D., Chen, S.-Y., Maksimchuk, A., Mourou, G., and Wagner, R., *Science*, **273**, 472 (1996).
3. Santala, M., Najmudin, Z., Tatarakis, M., Krushelnick, K., Dangor, A. E., Malka, V., Faure, J., Allott, R., and Clarke, R. J., *Phys. Rev. Lett.*, **86**, 1227 (2001).
4. Leemans, W. P., Rodgers, D., Catravas, P. E., Geddes, C. G. R., Fubiani, G., Esarey, E., Shadwick, B. A., Donahue, R., and Smith, A., *Phys. Plasmas*, **8**, 2510 (2001).
5. Schoenlein, R. W., Leemans, W. P., Chin, A. H., Volfbeyn, P., Glover, T. E., Balling, P., Zolotorev, M., Kim, K.-J., Chattopadhyay, S., and Shank, C. V., *Science*, **274**, 236 (1996).
6. Esarey, E., Shadwick, B. A., Catravas, P., and Leemans, W. P., *Phys. Rev. E*, **65**, 56505 (2002).
7. Wang, S., Clayton, C. E., Blue, B. E., Dodd, E. S., Marsh, K. A., Mori, W. B., Joshi, C., Lee, S., Muggli, P., Katsouleas, T., Decker, F. J., Hogan, M. J., Iverson, R. H., Raimondi, P., Walz, D., Siemann, R., and Assmann, R., *Phys. Rev. Lett.*, **88**, 135004 (2002).
8. Catravas, P., Esarey, E., and Leemans, W. P., *Phys. Plasmas*, **9**, 2428 (2002).
9. Dawson, J. M., *Phys. Rev.*, **133**, 383–387 (1959).
10. Tajima, T., and Dawson, J. M., *Phys. Rev. Lett.*, **43**, 267 (1979).
11. Litvak, A. G., *Zh. Eksp. Teor. Fiz.*, **57** (1969).
12. Max, C. E., Arons, J., and Langdon, A. B., *Phys. Rev. Lett.*, **33**, 209 (1974).
13. Kruer, W. L., *The physics of laser plasma interactions*, Addison-Wesley, New-York, 1988.
14. Antonsen, T. M., Jr., and Mora, P., *Phys. Rev. Lett.*, **69**, 2204–2207 (1992).
15. Sprangle, P., Esarey, E., Krall, J., and Joyce, G., *Phys. Rev. Lett.*, **69**, 2200 (1992).
16. Pukhov, A., Sheng, Z.-M., and ter Vehn, J. M., *Phys. Plasmas*, **6**, 2847 (1999).
17. Tsakiris, G. D., Gahn, C., and Tripathi, V. K., *Phys. Plasmas*, **7**, 3017–3030 (2000).
18. Gahn, C., Tsakiris, G. D., Pukhov, A., Meyer-ter-Vehn, J., Pretzler, G., Thirolf, P., Habs, D., and Witte, K. J., *Phys. Rev. Lett.*, **83**, 4772–4775 (1999).
19. Mendonça, J. T., *Phys. Rev. A*, **28**, 3592 (1983).
20. Sheng, Z.-M., Mima, K., Sentoku, Y., Jovanović, M. S., Taguchi, T., Zhang, J., and ter Vehn, J. M., *Phys. Rev. Lett.*, **88**, 55004 (2002).
21. Malka, V., Faure, J., Marquès, J.-R., Amiranoff, F., Rousseau, J.-P., Ranc, S., Chambaret, J.-P., Najmudin, Z., Walton, B., Mora, P., and Solodov, A., *Phys. Plasmas*, **8**, 0 (2001).
22. Mora, P., and Antonsen, T. M., Jr., *Phys. Plasmas*, **4**, 217–229 (1997).
23. Lefebvre, E., *Mécanismes d'absorption et d'émission dans l'interaction d'une impulsion laser ultra-intense avec une cible surcritique*, Thèse de doctorat, Université Paris XI Orsay (1996).
24. Faure, J., Marquès, J.-R., Malka, V., Amiranoff, F., Najmudin, Z., Walton, B., Rousseau, J.-P., Ranc, S., Solodov, A., and Mora, P., *Phys. Rev. E*, **63**, 654 (2001).
25. Faure, J., Malka, V., Marquès, J.-R., David, P.-G., Amiranoff, F., Phuoc, K. T., and Rousse, A., *Phys. Plasmas*, **9**, 756 (2002).
26. Mora, P., and Amiranoff, F., *J. Appl. Phys.*, **66**, 3476 (1989).
27. Esarey, E., Hafizi, B., Hubbard, R., and Ting, A., *Phys. Rev. Lett.*, **80**, 5552 (1998).